

Understanding the mechanisms of amorphous creep through molecular simulation

Penghui Cao^a, Michael P. Short^a, and Sidney Yip^{a,b,1}

^aDepartment of Nuclear Science and Engineering, Massachusetts Institute of Technology, Cambridge, MA 02139; and ^bDepartment of Materials Science and Engineering, Massachusetts Institute of Technology, Cambridge, MA 02139

Edited by Sharon C. Glotzer, University of Michigan, Ann Arbor, MI, and approved October 27, 2017 (received for review May 24, 2017)

Molecular processes of creep in metallic glass thin films are simulated at experimental timescales using a metadynamics-based atomistic method. Space-time evolutions of the atomic strains and nonaffine atom displacements are analyzed to reveal details of the atomic-level deformation and flow processes of amorphous creep in response to stress and thermal activations. From the simulation results, resolved spatially on the nanoscale and temporally over time increments of fractions of a second, we derive a mechanistic explanation of the well-known variation of creep rate with stress. We also construct a deformation map delineating the predominant regimes of diffusional creep at low stress and high temperature and deformational creep at high stress. Our findings validate the relevance of two original models of the mechanisms of amorphous plasticity: one focusing on atomic diffusion via free volume and the other focusing on stress-induced shear deformation. These processes are found to be nonlinearly coupled through dynamically heterogeneous fluctuations that characterize the slow dynamics of systems out of equilibrium.

creep | molecular simulation | deformation mechanism | atomistic modeling | metallic glass

Deformation and flow are fundamental in the rheological behavior of many materials (1–4). For the molecular understanding of plastic response under stress (creep), a standing challenge is to know the details by which the constituent atoms rearrange themselves individually and collectively in a local environment of stress and temperature. Creep experiments have been extensively reported on amorphous materials, including metallic glasses and colloidal systems (5–9). Yet, the relationship between stress and temperature effects on creep and the underlying microscopic processes remains an open question. Theoretical models have been proposed to describe the mechanisms of molecular deformation and flow responsible for amorphous plasticity. Spaepen (10) considered the distinction between homogeneous and inhomogeneous flows in metallic glasses and introduced the concept of the local free volume as an order parameter. In this view, local strain production and dissipation are assumed to be associated with individual atomic jumps. Argon (11) proposed a plastic deformation model of metallic glasses based on the notion of local shear transformations driven by stress and in the presence of thermal fluctuations. The atoms participating in such processes essentially undergo an inelastic shear deformation. Falk and Langer (12) later introduced the term shear transformation zone (STZ) in interpreting simulation results of viscoplastic deformation of amorphous solids. The STZ theory was further extended to be capable of describing temperature- and rate-dependent amorphous plasticity (13, 14). The term STZ has become widely adopted in studies of amorphous materials. (4, 8, 15–20).

We seek to identify the elementary processes of deformation and flow in amorphous creep through atomistic simulation. A bottleneck well-known in the literature is that the temporal scales relevant to creep are beyond the reach of traditional molecular dynamics (MD). To compensate for its inherently microscopic timescales, MD simulations of creep had to resort

to extreme conditions of stress, temperature, and strain rate (21, 22). Here, we implement a metadynamics formulation that allows transition-state trajectories to be generated on appreciably longer timescales on the order of fractions of seconds. By analyzing the distributions of atomic strain and nonaffine particle displacement, we observe the effects of stress and temperature on the evolution of activated states at the microscale. We find that the processes of single-particle diffusion and of shear deformation of small clusters of particles are both active in steady-state creep; in particular, their interplay gives rise to a characteristic upturn behavior of stress effects on creep rate. The simulation results also support a mechanism map showing a regime of low stress and high temperature where diffusional creep dominates and a high-stress regime governed by shear deformation creep. Our findings suggest that, while the two original models of amorphous plasticity (10, 11) are complementary in their individual focus, their combined effects need to be analyzed using more fundamental theories capable of treating the effects of nonlinear feedback.

Simulation Methods and Model

We consider a model $\text{Cu}_{50}\text{Zr}_{50}$ metallic glass system in two dimensions. The atoms interact through a Lennard–Jones potential (23, 24), which has been used to study plastic deformation (25) and thermally activated flows in metallic glass (26). Two amorphous structures with different sizes, 39.5×19.7 nm (containing 10,000 atoms) and 62.5×31.2 nm (25,000 atoms), are prepared by quenching from a high-temperature liquid state (*Materials and Methods* has additional details). We apply uniaxial tensile stress to the system and follow the procedure described in *Materials and Methods* to simulate the time evolution of creep.

Significance

The individual and collective molecular displacements in an amorphous solid undergoing plastic deformation are simulated by an atomistic method that allows incremental motions to be observed over a time window of fractions of seconds. Because the timescale matches well with the conditions of experimental measurements, simulation details provide dynamical evidence for the fundamental mechanisms of amorphous creep. In particular, knowledge of the interplay between diffusion (flow) and mechanical deformation processes enables us to explain the stress and temperature behavior of the experimental data as well as the validity of model descriptions of molecular mechanisms in terms of spatially and temporally heterogeneous fluctuations.

Author contributions: P.C. and S.Y. designed research; P.C. performed research; P.C., M.P.S., and S.Y. analyzed data; and P.C., M.P.S., and S.Y. wrote the paper.

The authors declare no conflict of interest.

This article is a PNAS Direct Submission.

Published under the PNAS license.

¹To whom correspondence should be addressed. Email: syip@mit.edu.

This article contains supporting information online at www.pnas.org/lookup/suppl/doi:10.1073/pnas.1708618114/-DCSupplemental.

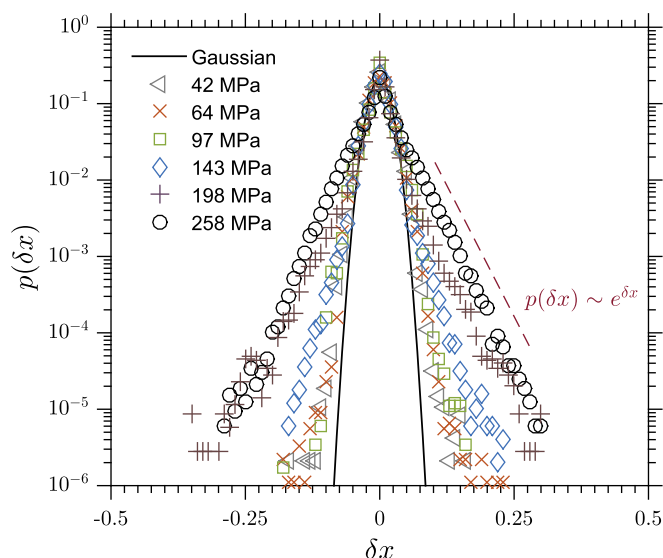


Fig. 3. Statistical distributions of nonaffine particle displacement $p(\delta x)$ at $0.68T_g$ and the various stresses indicated. The solid line represents the fitted Gaussian function, whereas the dashed line is exponential function used to guide the eye. The displacements δx are measured with a time interval of $\delta t = 0.01$ s.

of atoms involved in shear transformations is seen starting at a stress of 143 MPa. This suggests that stress plays a fundamental role in the physical manifestation of deformation and flow behavior in driven systems.

To see what molecular mechanisms could be associated with Figs. 3 and 4, we show in Fig. 5 the local space–time distributions. The spatial maps are resolved at the nanoscale and temporally measured over a time interval of 0.01 s. Maps of nonaffine displacements δx are shown in Fig. 5 *A* and *B*. Correspondingly, maps of D_{min}^2 (local deformation) are seen in Fig. 5 *C* and *D*. Fig. 5 *A* and *C* refers to low (64 MPa) stress, and Fig. 5 *B* and *D* for high (258 MPa) stress.

In Fig. 5A, the features of the nonaffine displacement map can be essentially attributed to thermally activated atomic diffusion, as initially proposed by Spaepen (10). It could serve as the baseline for measuring responses through single-particle displacements at higher stress. Fig. 5B indicates that the displacement magnitude of the sites of high mobility is about a factor of three larger than the displacements at low stress. Moreover, we see the presence of bidirectional flow (red–blue interface in Fig. 5B), as several such active zones appear along the 45° direction. When looking at Fig. 5D, these activated events appear as local strain bursts, a striking effect of stress-induced deformation. We regard this to be a specific simulation result, obtained at a physically meaningful timescale, that illustrates the synergistic effects of stress activation.

In Fig. 5C, we see little or no local shear deformation activity, which suggests that thermally diffusional rearrangements at the temperature of the simulation produce relatively small local plastic strain. These weak events seem quite random in space and do not align in any particular direction. We conclude that, at low stress, creep proceeds mostly by single-particle diffusion rather than cooperative atom deformation. However, at high stress, Fig. 5B and D implies that diffusive and deformation processes are both activated and coupled through heterogeneous stress fields in the driven system.

We apply the above findings to predict the variation of creep rate with tensile stress, a behavior of fundamental interest in the mechanics and physics of creep (30, 31). At very low stress, we expect the effects of thermal activation to dominate, which

should lead to a mild increase of creep rate with stress. As stress increases, both flow and deformation mechanisms contribute smoothly until the stress exceeds a threshold, at which point thermal and stress activations accelerate. The significant increase in shear transformation deformation events, shown in Fig. 4, *Inset* and the gap noted in Figs. 3 and 4, are hallmarks of a threshold (cross-over) behavior that is widely observed in experiments (Fig. 6B). We consider this stress threshold to reveal a regime of non-linear response, which has not been previously interpreted at the molecular level.

Creep Rate Upturn

The simulated creep curves allow us to determine a steady-state creep rate at each stress. Plotting the results in Fig. 64, we see a bimodal behavior in the monotonic variation of creep rate $\dot{\epsilon}$ with stress σ , a behavior visible in both the large and small systems. At low stress, $\dot{\epsilon}$ is characterized by a creep rate slope of $n \sim 1.5$, where n is known as the stress exponent. At high stress, n increases to ~ 5 . Notice that the stress value for the change in index n coincides with the stress gap mentioned in the discussions of Figs. 3 and 4. The transition in creep rate behavior is well-known in experiments on different materials (32–34). It is generally understood to signify thermal activation processes at low stress, changing over to stress activation for reasons that have not yet been resolved particularly regarding the roles of atomic diffusion and shear deformation.

To compare our results with experiments, the simulation data are shown again in Fig. 6B along with two sets of measurements (9, 33). Reduced stress σ/σ_0 and strain rate $\dot{\epsilon}/\dot{\epsilon}_0$ are plotted, where σ_0 and $\dot{\epsilon}_0$ are threshold values for creep rate upturn. The upturn in creep rate indicated by the simulation data matches well with the experiments. Our discussions concerning Figs. 3–5 lead us to interpret the creep rate behavior as evidence of the nonlinear response involving the coupling of the atomic diffusion and shear transformation deformation.

Creep Mechanism Map

The creep simulations that we have conducted cover three temperatures, 0.57, 0.68, and $0.91 T_g$, and stress values ranging

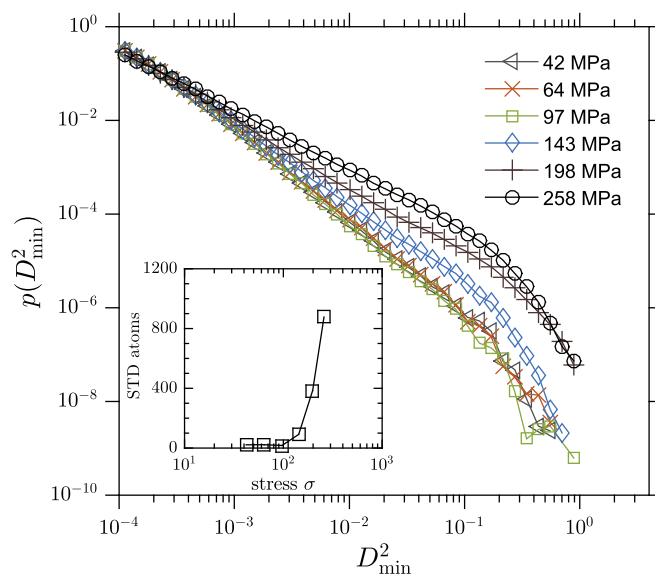


Fig. 4. Statistical distributions of deviatoric strain $p(D_{min}^2)$ at a temperature of $0.68T_g$ and the various stresses indicated. The strains are calculated with the time interval $\delta t = 0.01$ s. *Inset* shows variation of the number of shear transformation deformation (STD) atoms with strain that is larger than 0.05.

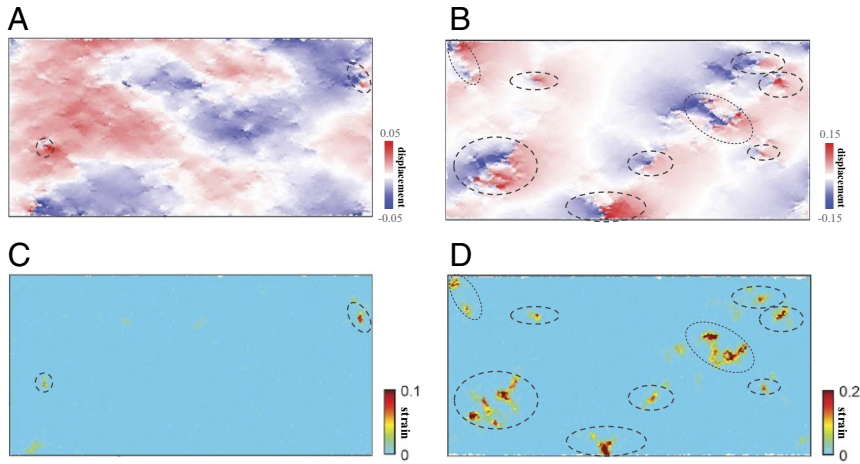


Fig. 5. Spatial distributions of nonaffine displacement (A and B) and of deviatoric strain (C and D). All measures are time incremental taken over a time interval of 0.01 s. Atoms are colored according to the magnitude of their displacements or strains. At each level, A and C denote low stress (64 MPa), and B and D denote high stress (258 MPa).

from 15 to 290 MPa. At each temperature, a stress-dependent creep rate (the rate for steady-state creep) curve was obtained, from which the stress exponent n was determined. The stress-temperature values of our simulations are plotted in Fig. 7 using squares and circles to denote whether the corresponding value of n is ~ 1 or > 5 , respectively. Fig. 7 is effectively a creep mechanism map for our model metallic glass. It delineates the stress-temperature regimes, where single-particle diffusion and shear transformation deformation are the limiting behaviors.

Looking at the simulation data across the temperature range, one can visualize a mechanism boundary separating the map into two domains, where either diffusion or shear deformation predominates. To motivate such a boundary, we recall well-known empirical expressions based on transition-state theory for the limiting behavior of strain rate in amorphous systems. At low stress, the creep rate $\dot{\epsilon}$ is written in the form (10)

$$\dot{\epsilon} = \gamma_0 \cdot \exp\left(-\frac{Q_d}{kT}\right) \frac{V_d}{kT} \sigma, \quad [1]$$

where Q_d and V_d are the activation energy and activation volume for diffusion, respectively. This is derived based on the free volume diffusion model. At high stress, a more appropriate form is (8, 11)

$$\dot{\epsilon} = \gamma_0 \cdot \exp\left(-\frac{Q_{st} - \sigma V_{st}}{kT}\right), \quad [2]$$

where the subscript st denotes shear transformation. This is compatible with the shear transformation deformation model. Setting Eq. 1 equal to Eq. 2 and treating these activation parameters numerically, we find the locus of (σ, T) values for the mechanism boundary to be essentially a straight line: $\sigma(T) = a + bT$ (Supporting Information has details). The red dashed curve in Fig. 7 is drawn having this functional form and adjusted to separate the groups of squares and circles. Thus, the simulation data are able to accommodate a boundary that would have the two limiting behaviors described by Eqs. 1 and 2.

For experimental validation, we show in Fig. 7 mechanical deformation measurements on a five-component metallic glass (9). Except for an overall shift, the experimental and simulation results both display the same predominant domains of diffusional and deformational creep. One can offer only qualitative reasons why a comparison between this simulation and experiment should be considered meaningful. For example, differences between the simulation system and the experimental samples can be quite significant. These could arise from their respective preparations, such as cooling rate and casting defects and surface polish imperfections. Another factor is that an idealized 2D binary mixture model is being compared with measurements on

a 3D five-component material. Although a 2D model could be capable of capturing aspects of thermally activated diffusion and stress-induced shear transformation processes, one could argue that the system dimensionality could affect activation energy

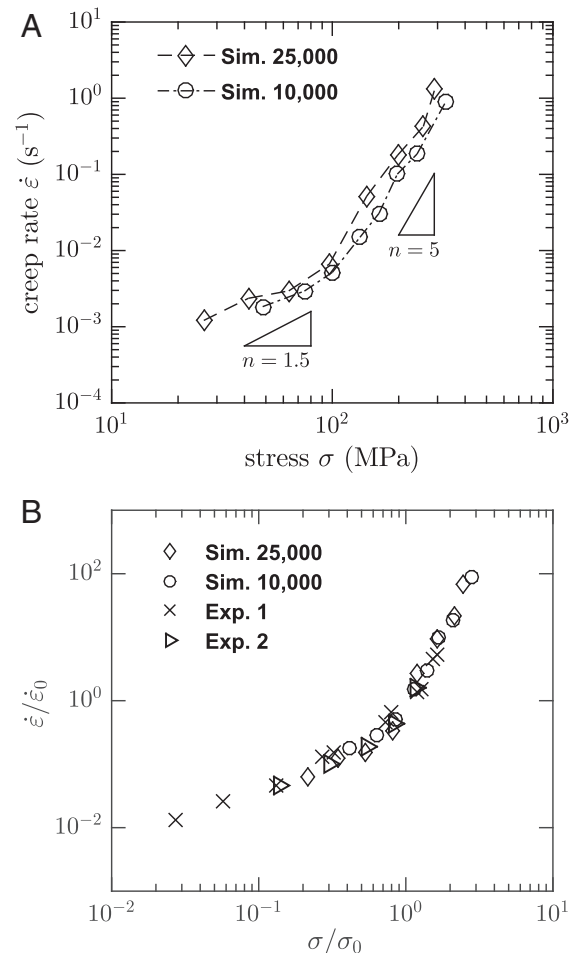


Fig. 6. (A) Stress dependence of creep rate from simulations with two different system sizes of 25,000 and 10,000 atoms. (B) Stress variation of creep rate. The two sets of experimental data 1 (crosses) and 2 (triangles) are adapted from refs. 9 and 33, respectively; σ_0 and $\dot{\epsilon}_0$ are threshold values in the creep rate-stress curve.

as measures of local plastic deformation (12, 52). Imagine that a region surrounding an atom undergoes a strain deformation during a time interval δt . The deviatoric strain is defined as

$$D_{min}^2(\delta t) = \sum_{i=1}^n [\mathbf{X}_i(t + \delta t) - \mathbf{X}_0(t + \delta t) - \mathbf{J} \times (\mathbf{X}_i(t) - \mathbf{X}_0(t))]^2, \quad [3]$$

where $\mathbf{X}(t)$ is the reference configuration at time t , $\mathbf{X}(t + \delta t)$ is the current configuration at time $t + \delta t$, and the index i runs over all atoms within the interaction cutoff relative to the reference position of atom zero. \mathbf{J} is the affine deformation tensor that transforms a nearest neighbor separation, $\mathbf{X}_i(t) - \mathbf{X}_0(t)$, to what would be expected under an affine deformation. The deformation tensor \mathbf{J} is determined by minimizing D_{min}^2 with the minimum value being the atomic-level deviatoric strain. For each \mathbf{J} , a Green strain tensor η can be written as $\eta = 1/2(\mathbf{J} + \mathbf{J}^T - \mathbf{I})$. The local atomic strain invariant η_{Mises} in two dimensions is computed by

$$\eta_{Mises} = \sqrt{\eta_{xy}^2 + \frac{\eta_{xx}^2 + \eta_{yy}^2 - \eta_{xx}\eta_{yy}}{3}}. \quad [4]$$

Note that η_{Mises} is directly derived from \mathbf{J} , while D_{min}^2 is a measure of the deviation from deformation tensor \mathbf{J} . The atomic strains η_{Mises} and D_{min}^2 are

computed by considering all of the n neighboring atoms. Both can serve as an indicator for cooperative local rearrangement.

The nonaffine displacement is useful for tracking single-atom dynamics. For a time interval $(t, t + \delta t)$, it is defined as

$$\delta u_{\alpha}(t, t + \delta t) = X_{\alpha}(t + \delta t) - F_{\alpha\beta} X_{\beta}(t), \quad [5]$$

where the Greek indices α and β indicate the Cartesian components and the deformation gradient F is related to the system-level creep strain $\varepsilon_{\alpha\beta}$ by $F_{\alpha\beta} = 1 + [\varepsilon_{\alpha\beta}(t + \delta t) - \varepsilon_{\alpha\beta}(t)] = 1 + \Delta\varepsilon_{\alpha\beta}(t, t + \delta t)$. In the simulation, the nonaffine displacement in the tensile direction δx is calculated for characterization of single-atom dynamics.

ACKNOWLEDGMENTS. We thank A. S. Argon, J. S. Langer, and K. Kamrin for discussions, and the Massachusetts Institute of Technology (MIT) Nuclear Science and Engineering Department for computational resources. P.C. was supported by US Department of Energy (DOE) Grant DE-NE0008450. M.P.S. was supported by National Science Foundation CAREER Grant DMR-1654548. S.Y. was supported by DOE-Basic Energy Sciences Grant DE-SC0002633 and the Kuwait-MIT Center Signature Project. S.Y. is a founding member of the MIT Concrete Sustainability Hub.

- Mason T, Bibette J, Weitz D (1996) Yielding and flow of monodisperse emulsions. *J Colloid Interface Sci* 179:439–448.
- Johnson WL, Lu J, Demetriou MD (2002) Deformation and flow in bulk metallic glasses and deeply undercooled glass forming liquids—a self consistent dynamic free volume model. *Intermetallics* 10:1039–1046.
- Debregeas G, Tabuteau H, Di Meglio JM (2001) Deformation and flow of a two-dimensional foam under continuous shear. *Phys Rev Lett* 87:178305.
- Schall P, Weitz DA, Spaepen F (2007) Structural rearrangements that govern flow in colloidal glasses. *Science* 318:1895–1899.
- Krispeneit JO, et al. (2014) Crossover from random three-dimensional avalanches to correlated nano shear bands in metallic glasses. *Nat Commun* 5:3616.
- Huang Y, Shen J, Chiu Y, Chen J, Sun J (2009) Indentation creep of an Fe-based bulk metallic glass. *Intermetallics* 17:190–194.
- Siebenbürger M, Ballauff M, Voigtman T (2012) Creep in colloidal glasses. *Phys Rev Lett* 108:255701.
- Schuh CA, Hufnagel TC, Ramamurty U (2007) Mechanical behavior of amorphous alloys. *Acta Mater* 55:4067–4109.
- Lu J, Ravichandran G, Johnson WL (2003) Deformation behavior of the Zr 41.2 Ti 13.8 Cu 12.5 Ni 10 Be 22.5 bulk metallic glass over a wide range of strain-rates and temperatures. *Acta Mater* 51:3429–3443.
- Spaepen F (1977) A microscopic mechanism for steady state inhomogeneous flow in metallic glasses. *Acta Metall* 25:407–415.
- Argon AS (1979) Plastic deformation in metallic glasses. *Acta Metall* 27:47–58.
- Falk ML, Langer JS (1998) Dynamics of viscoplastic deformation in amorphous solids. *Phys Rev E* 57:7192–7205.
- Falk M, Langer J, Pechenik L (2004) Thermal effects in the shear-transformation-zone theory of amorphous plasticity: Comparisons to metallic glass data. *Phys Rev E* 70:011507.
- Bouchbinder E, Langer J (2009) Nonequilibrium thermodynamics of driven amorphous materials. II. Effective-temperature theory. *Phys Rev E* 80:031132.
- Mayr S (2006) Activation energy of shear transformation zones: A key for understanding rheology of glasses and liquids. *Phys Rev Lett* 97:195501.
- Tanguy A, Leonforte F, Barrat JL (2006) Plastic response of a 2D Lennard-Jones amorphous solid: Detailed analysis of the local rearrangements at very slow strain rate. *Eur Phys J E* 20:355–364.
- Pan D, Inoue A, Sakurai T, Chen M (2008) Experimental characterization of shear transformation zones for plastic flow of bulk metallic glasses. *Proc Natl Acad Sci USA* 105:14769–14772.
- Cao P, Park HS, Lin X (2013) Strain-rate and temperature-driven transition in the shear transformation zone for two-dimensional amorphous solids. *Phys Rev E* 88:042404.
- Greer A, Cheng Y, Ma E (2013) Shear bands in metallic glasses. *Mater Sci Eng R Rep* 74:71–132.
- Cao P, Lin X, Park HS (2014) Surface shear-transformation zones in amorphous solids. *Phys Rev E* 90:012311.
- Yamakov V, Wolf D, Phillpot SR, Mukherjee AK, Gleiter H (2002) Dislocation processes in the deformation of nanocrystalline aluminium by molecular-dynamics simulation. *Nat Mater* 1:45–49.
- Sentjabrskaja T, et al. (2015) Creep and flow of glasses: Strain response linked to the spatial distribution of dynamical heterogeneities. *Sci Rep* 5:11884.
- Kobayashi S, Maeda K, Takeuchi S (1980) Computer simulation of deformation of amorphous Cu57Zr43. *Acta Metall* 28:1641–1652.
- Deng D, Argon A, Yip S (1989) A molecular dynamics model of melting and glass transition in an idealized two-dimensional material I. *Philos Trans R Math Phys Eng Sci* 329:549–573.
- Schuh CA, Lund AC (2003) Atomistic basis for the plastic yield criterion of metallic glass. *Nat Mater* 2:449–452.
- Rodney D, Schuh C (2009) Distribution of thermally activated plastic events in a flowing glass. *Phys Rev Lett* 102:235503.
- Cao A, Cheng Y, Ma E (2009) Structural processes that initiate shear localization in metallic glass. *Acta Mater* 57:5146–5155.
- Chaudhuri P, Berthier L, Kob W (2007) Universal nature of particle displacements close to glass and jamming transitions. *Phys Rev Lett* 99:060604.
- Weeks ER, Crocker JC, Levitt AC, Schofield A, Weitz DA (2000) Three-dimensional direct imaging of structural relaxation near the colloidal glass transition. *Science* 287:627–631.
- Cottrell AH (1953) *Dislocations and Plastic Flow in Crystals* (Clarendon, Oxford).
- Nabarro FRN, De Villiers F (1995) *Physics of Creep and Creep-Resistant Alloys* (CRC, Boca Raton, FL).
- Boyle JT, Spence J (2013) *Stress Analysis for Creep* (Elsevier, Amsterdam).
- Nieh T, Wadsworth J (2006) Homogeneous deformation of bulk metallic glasses. *Scr Mater* 54:387–392.
- Clueh R (2005) Elevated temperature ferritic and martensitic steels and their application to future nuclear reactors. *Int Mater Rev* 50:287–310.
- Cheng Y, Ma E (2011) Atomic-level structure and structure–property relationship in metallic glasses. *Prog Mater Sci* 56:379–473.
- Falk ML, Langer JS (2011) Deformation and failure of amorphous, solidlike materials. *Annu Rev Condens Matter Phys* 2:353–373.
- Langer J (2015) Shear-transformation-zone theory of yielding in athermal amorphous materials. *Phys Rev E* 92:012318.
- Hufnagel TC, Schuh CA, Falk ML (2016) Deformation of metallic glasses: Recent developments in theory, simulations, and experiments. *Acta Mater* 109:375–393.
- Langer J (2017) Yielding transitions and grain-size effects in dislocation theory. *Phys Rev E* 95:033004.
- Kamrin K, Bouchbinder E (2014) Two-temperature continuum thermomechanics of deforming amorphous solids. *J Mech Phys Sol* 73:269–288.
- Chatteraj J, Caroli C, Lemaître A (2010) Universal additive effect of temperature on the rheology of amorphous solids. *Phys Rev Lett* 105:266001.
- Kob W, Donati C, Plimpton SJ, Poole PH, Glotzer SC (1997) Dynamical heterogeneities in a supercooled Lennard-Jones liquid. *Phys Rev Lett* 79:2827–2830.
- Hoffmann S, et al. (2000) Origin of dynamic heterogeneities in miscible polymer blends: A quasielastic neutron scattering study. *Phys Rev Lett* 85:772–775.
- Becker T, Smith JC (2003) Energy resolution and dynamical heterogeneity effects on elastic incoherent neutron scattering from molecular systems. *Phys Rev E* 67:021904.
- Jensen HJ (1998) *Self-Organized Criticality: Emergent Complex Behavior in Physical and Biological Systems* (Cambridge Univ Press, Cambridge, UK), p 126.
- Gruber M, Abade GC, Puertas AM, Fuchs M (2016) Active microrheology in a colloidal glass. *Phys Rev E* 94:042602.
- Antonaglia J, et al. (2014) Bulk metallic glasses deform via slip avalanches. *Phys Rev Lett* 112:155501.
- Fan Y, Yildiz B, Yip S (2013) Analogy between glass rheology and crystal plasticity: Yielding at high strain rate. *Soft Matter* 9:9511–9514.
- Kushima A, et al. (2009) Computing the viscosity of supercooled liquids. *J Chem Phys* 130:224504.
- Cao P, Li M, Heugle RJ, Park HS, Lin X (2012) A self-learning metabasin escape algorithm and the metabasin correlation length of supercooled liquids. *Phys Rev E* 86:016710.
- Henkelman G, Uberuaga B, Jonsson H (2000) A climbing image nudged elastic band method for finding saddle points and minimum energy paths. *J Chem Phys* 113:9901–9904.
- Shimizu F, Ogata S, Li J (2007) Theory of shear banding in metallic glasses and molecular dynamics calculations. *Mater Trans* 48:2923–2927.